IEEE Access
Multidisciplinary ⋮ Rapid Review ⋮ Open Access Journal

Received 16 February 2024, accepted 13 March 2024, date of publication 19 March 2024, date of current version 1 May 2024.

Digital Object Identifier 10.1109/ACCESS.2024.3379272

RESEARCH ARTICLE

Harnessing the Potential of High-Efficiency Synchronous Generators in Wind Energy Conversion Systems

AMINA MSEDDI[1,2], AHMED ABID[1,2], OMAR NAIFAR[1], MOHAMED RHAIMA[3], ABDELLATIF BEN MAKHLOUF[4], AND LASSAAD MCHIRI[5]

[1]Control and Energy Management Laboratory, National School of Engineering, University of Sfax, Sfax 3038, Tunisia
[2]Renewable Energy Department, ISE Company, Sfax 3041, Tunisia
[3]Department of Statistics and Operations Research, College of Science, King Saud University, Riyadh 11451, Saudi Arabia
[4]Department of Mathematics, Faculty of Sciences of Sfax, University of Sfax, Sfax 3038, Tunisia
[5]Department of Mathematics, Panthéon-Assas University Paris II, 75006 Paris, France

Corresponding author: Omar Naifar (omar.naifar@enis.tn)

This research was funded by King Saud University in Riyadh, Saudi Arabia through researchers supporting project number (RSPD2024R683).

ABSTRACT Dual Excitation Generators (DESGs) are a potential improvement in high-efficiency generator technology, but optimizing performance and control techniques remains a difficulty. This work focuses on a detailed examination of a 1.5 MW DESG, with the goal of identifying important electrical features for optimal control implementation using an analytical sizing method. The project also intends to present and evaluate a novel control mechanism, the Fractional Order Proportional Integral (FOPI) controller. The inquiry begins with a comprehensive literature analysis that categorizes DESGs and describes their many uses. Using experimental data, a custom mathematical model integrating spatial harmonics is created to improve model precision. The FOPI controller is then introduced and tested using simulations with the NREL lab's Fatigue Aerodynamic Structure and Turbulence (FAST) program. The study's findings show significant development in wind energy control systems, notably in terms of improving power extraction and velocity tracking. The FOPI controller appears as a revolutionary technology, providing greater stability and robustness in DESG control over its operating range.

INDEX TERMS Advanced modeling, analytical sizing, DESG, robust control, wind conversion system.

I. INTRODUCTION

Renewable energy, particularly wind energy, is gaining traction as a viable alternative to traditional energy sources due to its low carbon footprint and long-term viability.

Recent research by [1] has emphasized the possibility of innovative blade designs to improve wind turbine efficiency by maximizing aerodynamic performance. Reference [2] have illustrated how improved control algorithms may improve wind energy system performance and grid integration. Reference [3] have also recently concentrated on new materials and manufacturing processes to improve the efficiency and reliability of wind turbine components. Furthermore, [4] and [5]investigated the integration of energy storage systems with wind farms to improve grid stability and increase energy consumption. Finally, [6] describe improvements in offshore wind technology as potential prospects for enhancing the efficiency and scalability of wind energy conversion systems. However, there is no agreement on the ideal design for future wind generators, the trend appears to be toward Synchronous Machines (SM). Permanent Magnets (PM) or Wound Rotors (WR). Recent advances in wind energy conversion have resulted in the development of high-efficiency generators aimed at improving the performance of wind turbine systems. For example, current research on doubly-fed induction technology, particularly in terms of generator control techniques [7], [8], [9], has sparked widespread interest. These investigations have looked at the capabilities and benefits of this technology as

The associate editor coordinating the review of this manuscript and approving it for publication was Javed Iqbal.

a high-efficiency generator within wind energy conversion systems (WECS).

Furthermore, [10] suggested a high-efficiency wind turbine generator based on a permanent magnet synchronous machine with Open-Winding, which showed promising energy conversion efficiency. Similarly, [11] presented a revolutionary new design of a high-efficiency permanent magnet generator designed specifically for wind energy conversion systems, demonstrating increases in both efficiency and reliability.

Permanent magnets generators have various advantages over rotor windings, including greater efficiency since the rotor's loss of copper is eliminated, grater power density, and quicker response because of their small mechanical time constant. Regarding to the speed control, it may be controlled by acting on the excitation flux ϕ_{ext}. However, because this flux is continuous, power electronics are employed to deflux electricity. This solution is the core of the double-excited synchronous machine (DESM) described and utilized in this research. Dual excitation generators have emerged as a potential technology for wind energy conversion systems in this area.

When compared to a traditional machine as a wound rotor machine (WRM), this form of equipment may be more efficient [13] even for high operating temperatures. In addition, they have a lower harmonic rate. A flux concentration rotor with ferrite PM is another advantage of this structure: on one side, the quantity of the PMs is reduced in comparison to traditional permanent magnet machines (PMM), so the machine is cheaper. The addition of PM, on the other side, increases the generator's performance. Furthermore, the addition of the of Excitation Coils (EC) make the Excitation Flux (EF) controllable. This later may be raised/lowered by changing the direction of the DC excitation current throughout a large velocity interval.

In generator mode, double-excited synchronous generator linked to a PD3 rectifier are a viable option to PM machines associated to a full charge power converter. Furthermore, this double excitation allows a high rotation speed in motor mode, and the use of PM promotes energy efficiency [14]. Even with a half load, the machine may function at peak efficiency. Other machine topologies make this difficult to achieve [15]

In this work, the authors focus on the development of a 1.5MW dual excitation generator system for wind energy conversion that outperforms existing wind turbines in terms of performance and efficiency for the following reasons:

- HESMs are more efficient than WRSMs, even at high temperatures,
- HESM have a lower frequency of harmonics than the WRSM,
- The use of a flux-concentrating rotor with ferrite PM reduces the size of the magnets compared to conventional PM machines,
- HESM have lower cost,
- The use of magnets improves the performance and compactness (torque/mass and power/mass ratios) of a generator,
- The utilization of field coils allows for higher flux control than permanent magnet synchronous machines,

One significant addition of our research is the step-by-step modeling of the DESG, which fills a critical gap in the previous literature. Because this generator is not readily accessible in MATLAB Simulink, researchers must model it separately. By offering a complete modeling approach, the behavior of the DESG under a variety of operating circumstances maybe tested and investigated. Furthermore, we thoroughly documented the DESG's control mechanism, which extended from the inner loop of DC excitation current to the outer loop of speed regulation. Our findings show great electrical performance, including speed monitoring, while also solving mechanical issues like decreasing shaft torsion fatigue.

These results were compared to existing literature, namely wind turbines like WindPACT (WP) turbine [16].

To sum up the main contributions of our research may be summarized as follows:

- Extensive survey of the literature on hybrid/double excitation machines is offered. The structural topology and operating principles of the hybrid excitation machine are then investigated.
- Detailed mathematical model for DESGs is developed based on experimental data is introduced.
- Introduction of a reliable and straightforward analytical sizing approach for determining the optimal generator size for a particular WECS.
- For the first time in the literature, a FOPI is evaluated on a 1.5MW wind conversion system to enhance the electrical management, to reduce mechanical vibration: a comparison with an antiwindup gain scheduled PID controller presented in previous works and conducted under the same wind turbine is performed.

Beginning with an overview of DESGs, this paper categorizes and evaluates their structure and use, highlighting their novel design characteristics. The focus then moves to an investigation of DESG's possibilities in WECS, including generator and control strategy selection. The study then discusses an analytical sizing strategy for a 1.5 MW DESG, followed by thorough modeling approaches that account for space harmonics. The electrical control of the wind system is described, including current and speed loop control schemes and simulation results.

II. OVERVIEW OF HESM

A. USE, TYPE, AND STRUCTURE OF DESG

As previously mentioned, the usage of permanent magnets as opposed to rotor windings can provide considerable benefits, such as increased efficiency owing to the elimination of copper loss, increased power density, and quicker reaction thanks to the low electromechanical time constant. However, the principal flux produced by the permanent magnet cannot be

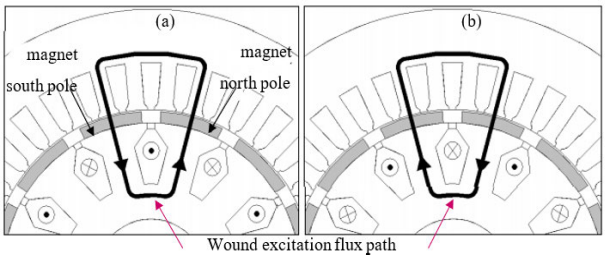

FIGURE 1. Flux variation: (a) Flux increase (b) Flux reduction [17].

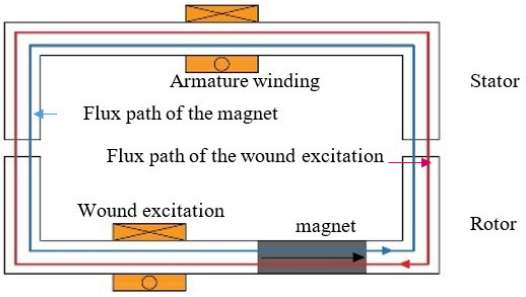

FIGURE 2. Schematic diagram of a series HESM.

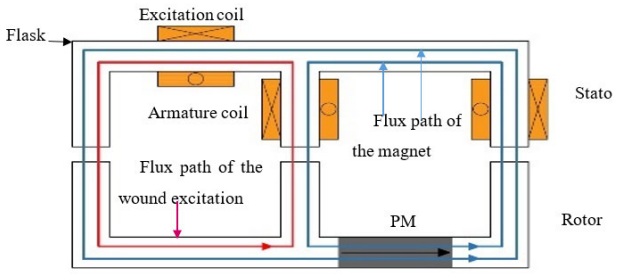

FIGURE 3. Operating principle of a unipolar HESM.

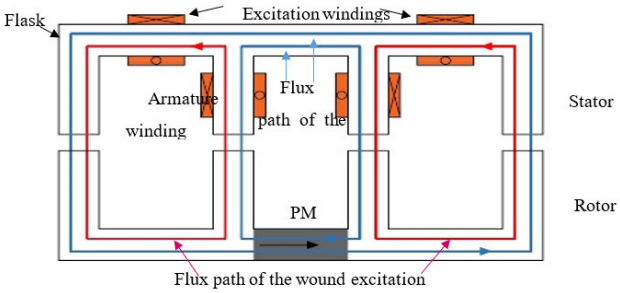

FIGURE 4. Operating principle of the bipolar HESM.

adjusted, which is the primary downside of this machine type. In this paragraph, we will define, classify and give the most relevant utilization and designs of a DESG in the literature.

1) DEFINITION

The concept of double-excitation synchronous machine (DESM) is present in many works.

Different terms qualify this type of machine in the literature [14]:

- Hybrid excitation synchronous machines;
- Dual excitation synchronous machines or Double excitation synchronous machines;
- Combined excitation synchronous machines;
- Permanent magnet synchronous machines with exciting auxiliary windings.

The excitation flux can be intensified or reduced by changing the direction of the continuous excitation current over a broad range of velocity (Figure.1).

2) CLASSIFICATION OF HESM

There are generally three ways to classify HESM.

- The first one is related to the location of the flow sources in the machine [14], [18]:
  - ✓ Excitation sources on the rotor (SER).
  - ✓ Excitation sources on the stator (SES).
  - ✓ Mixed excitation sources (SEM).

  To improve reliability, the two excitations should be located on the side of the stator. This would require simpler analysis and manufacturing, fewer protective measures, and provide better upshift capability. Such a configuration would also avoid slippery contacts. However, in this case, the design of this structure is complex.
- The second one is related to the trajectory of the magnetic field: 2D or 3D evolution.
- The last one is related the combination of the two excitation sources: series or parallel [14]. In this work, we choose to classify the HESM according to the third criterion.

a: HESM SERIES

Here, the flux of the wound excitation crosses that of the permanent magnets. The schematic diagram is that of FIGURE 2.

In this figure, the total flux is subtractive because the flux from the magnet is opposite to the flux from the coil excitation, resulting in a decrease in the total magnetic induction. However, it is possible to have an additive flux.

Since the PM have a permeability close to air, the coils have a high reluctance (air gap + magnets). For their defluxing, an important excitation current must be injected, which increases the Joule losses in the inductor. Obviously, a good dimensioning of the machine will allow a good operation of the wound de-excitation. On the other hand, another disadvantage of this structure is that it can lead to demagnetization of the magnets [15].

b: PARALLEL HESM

The path of the excitation flux created by the excitation coils is different from that created by the magnets, it does not pass through them. There is therefore no risk of demagnetization of the magnets by the excitation coils. The magnetic flux of this machine evolves in 3D. A parallel HESM can be unipolar or bipolar.

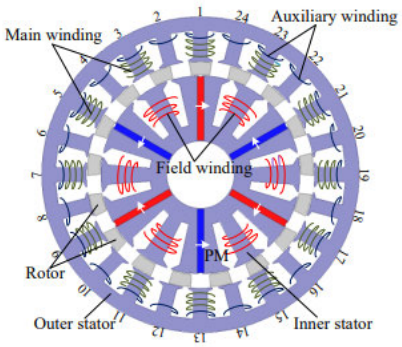

FIGURE 5. Topology proposed by [22].

i) UNIPOLAR HESM

The schematic diagram is given by FIGURE 3.

This structure is more efficient than the series HESM, since the excitation flux does not pass through the magnets, but the flux compensation is not total. The excitation flux has a positive DC component since one of the poles is not compensated. There is therefore the possibility that the iron losses are not reduced for all operating points [15], [19]. Reducing the excitation flux is easy, but increasing it is difficult. Another problem is present in this structure: the flanges make the flux created by the magnets lower than for a PMSM with the same volume of PM.

ii) BIPOLAR HESM

In FIGURE 4, the flux of the excitation winding acts on both poles.

This structure has the same disadvantages as those mentioned above: the flanges mean that the flux created by the magnets is lower than a PMSM with the same volume of PM and the flux compensation is not total. The advantage of this architecture compared to the unipolar HESM is that it is possible to add or subtract the excitation flux freely.

3) DESG INNOVATIVE DESIGN REVIEW

The work carried out in [20], [22] focused on the design aspect of the HESM without specifying a particular application area. The goal was essentially to improve the electromagnetic performance.

The authors of [20] selected certain structural parameters to optimize the proposed HESM. They played with a number of rotor and stator parameters such as rotor outer radius, pole height and width; stator pole height and width; field winding slot width and core height; permanent magnet width and length…As a result, they achieved a much higher no-load electromotive force, lower torque ripple, and greater flux decay capability.

In [21], the new hybrid machine is obtained by using the flux of the magnets to counteract the excitation flux and by inserting PM between the poles of the stator. The electromagnetic characteristics of the machine were analyzed at no-load and under load by a FEA and experimentally. The new topology was developed based on the principle of the flux-commutated machine (FCM), a comparison of the electromagnetic torques and losses was performed for both machines. The results show an increase by 18% of the mean electromagnetic torque of the considered machine (for a fixed copper loss) compared to that of the FMC due to the reduction of magnetic saturation in the stator.

Finally, the configuration proposed in [22] consists of two separate stators and a rotor sliced into a ''sandwich'' as shown in FIGURE 5.

Two armature windings are arranged to perform tow functions. The first one consists of the flux decay. The second function consists of recycling the magnetic energy which is generated during field regulation. These windings have different numbers of pole pairs. A finite element analysis and experimental investigation on a laboratory prototype proved the feasibility of this new hybrid solution. proved that the increase the output torque and power of HESMs for high operating speeds is effective by using the recycled energy.

Most of the work presented in this section has focused on the design, fabrication, and testing of HESMs. Few references study the control aspect and robust regulation of the HESM. It is this aspect that is developed in our work.

B. UTILIZATION

In the last few years, a lot of work has been done on transmission systems as well as on power generation systems (such as wind power) applied to energy conservation. In this context, HESMs are of great interest and have become an important research topic. More than 19000 scientific papers have been published in the last ten years on these machines. Its fields of application are multiple.

1) MOTOR APPLICATION

So far, the applicability of this machine has been proved in motor mode. It has been widely investigated in traction applications [20], [23]. Indeed, a motor designed for an electric vehicle requires a high starting torque, an acceptable efficiency and a large speed range. In this field, the work carried out in [19] and [24] proposed a new conception of the HESM. The results presented in [19] proved that the torque ripple of the machine could be minimized by the coordinated operation between the field current and the armature current. A 100kW hybrid motor was fabricated to perform experimental investigation. The applicability of the HESM in the field of traction for electric vehicles have thus been experimentally validated.

In [25], the authors showed that, compared to PMSM, HESM may decrease the flux without raising the armature current for an electric traction application. In addition, it has the advantage of a flexible design. In fact, in PMSMs, to increase the operating speed range, the flux must be decreased for high rotation speeds. This is achieved by demagnetizing the PM by adjusting (increasing) the direct axial current, which permanently creates the risk of their

demagnetization. In addition, this additional direct axial current leads to high Joule losses.

Apart from the design aspect, research has focused on the control aspect of the hybrid machine in the field of electric traction [26], [27] and railway traction [28]. In [26], a hybrid excitation machine with an open winding structure is presented. The purpose of this research is to realize the power distribution control between the battery and the motor in the powertrain of a hybrid electric vehicle (HEV). The feasibility and the effectiveness of the power distribution control scheme using a hybrid machine was proved by simulation.

Reference [28] compared the performance of an HESM and a PMSM with similar configurations in the railway traction domain. The results showed that, for a train driving cycle with a reduced operating speed range, the PMSM provides better performance. However, as the speed range increases, the HESM has better performance compared to the PMSM, especially in terms of loss minimization at the expense of higher volume and cost. The advantage of the HESM's continuous excitation windings is most remarkable at high rotation speeds, where it is difficult for a PMSM to maintain a low flux in the air gap.

2) GENERATOR APPLICATION

A number of works have proposed the use of HESM in generator mode, in applications such as marine [13], [29] small hydroelectric power plants [30] and aeronautics [31], [32].

In [29], the performance of the HESM compared to the PMSM is proven by a finite element analysis (FEA). For the application under consideration (marine diesel generator), the generator voltage must be maintained within ±10% of its nominal value and the short-circuit current must be at least three times the nominal current for at least two seconds. This second condition is a major problem for PMSM.

In [30], The authors compared the performance of a dual-excitation synchronous machine to that of a wound-excitation SM and to that of the PMSM. They showed that, compared to the wound-excitation SM, for a hydroelectric plant, the HESM had a much higher efficiency. The stator copper losses are a little higher (due to the length of the HESM stator) but the rotor copper losses are much lower, which shows the efficiency of the hybrid generator compared to the wound excitation MS. For a unit power factor, the efficiencies of the PMSM and HESM are comparable.

For aircraft on-board power supply, [32]has shown that the DESG is a competitor to the three-stage synchronous machine currently used in most commercial and military aircraft power systems [33] because of its higher power density, simpler structure and more compact size.

Several research on the usage of DESGs in WECSs have been undertaken, with many concentrating on the design, control, and optimization of DESGs for optimal performance. In this sector, the GREYC team in France [34]suggests using a DESG by connecting it to the grid via a three-stage power

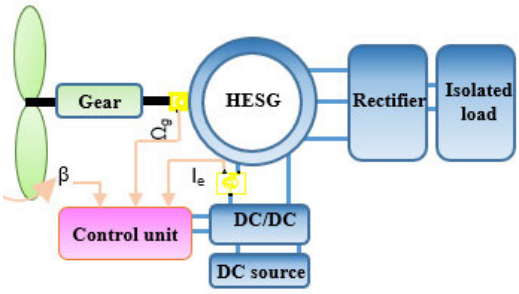

FIGURE 6. WECS architecture.

electronics system (AC/DC/AC converter). Another research, this time at the L2EP laboratory in France, emphasized the mass and energy efficiency of this generator for high power applications, particularly wind generation, when compared to the salient pole synchronous generator (SPSG) [17]. The authors investigated how different DESG design characteristics, such as stator and rotor size, winding topologies, and magnetic material qualities, affected WECS effectiveness. [35] created a control technique for a DESG-based WECS that maximized power production by optimizing generator torque and speed.

Other research has concentrated on the incorporation of DESGs into WECSs and the possible benefits of integrating DESGs in various WECS applications. For example, [36] designed and modeled a 1.5 MW grid-connected WCES based on a DESG. The authors examined the performance of a DESG-based WECS in both grid-connected and standalone modes, demonstrating that the DESG system was extremely efficient and dependable in both cases.

Reference [37]explored the usage of DESGs in offshore wind farms, demonstrating that DESGs may drastically reduce generator size and weight while improving overall system efficiency.

Reference [38] presented a new DESG design with a dual-stator layout to increase efficiency and save costs.

Despite these advancements, there are still significant obstacles to overcome in the usage of DESGs in WECSs. These include DESG control, system stability, and cost-effectiveness problems. Our research seeks to contribute to this field by providing an overview of the possibilities of DESG technology in WECSs, as well as emphasizing the particular benefits and problems connected with this technology.

In summary, the existing literature on DESG in WECSs has demonstrated the potential of this technology for improving the performance and efficiency of WECSs. This study builds on this knowledge by providing a comprehensive overview of DESG technology and its potential applications in WECSs.

III. DESG POTENTIAL IN WECS

In this work two axes have been privileged which are the choice of the wind generator and its control strategy.

A. CHOICE OF THE GENERATOR

Previous works dealt with the dual excitation synchronous generator based WECS. In [34], the MPPT is ensured by an inverter which controls the generators' stator currents. The adjustment of the stator currents enables to track the optimal rotation speed. However, using an inverter for MPPT increases the cost of the WECS because the rotation speed may be easily controlled by manipulating the DC excitation winding. By adopting this architecture, the full-scale power converter (inverter) is simply replaced by a chopper. The power of this later doesn't exceed 10% of the total generator power. Compared to conventional PMSGs, the dual excitation synchronous generator allows a flexible flux control through continuous excitation windings. That is to say, there is no need of complex power convertors to control the rotation speed of the generator. A simple chopper can suffice. However, the regulation of a hybrid generator has a significant disadvantage. Indeed, dual excitation synchronous generator are highly non-linear. Therefore, it is necessary to use robust controllers.

Finally, the proposed simple architecture of the WT system is presented in FIGURE 6.

Indeed, the dual excitation variable speed synchronous generator is driven by a horizontal axis WT. A chopper supplies the excitation windings of the generator. This later feed a resistive isolated load via a rectifier.

B. CHOICE OF THE CONTROL STRATEGY

Until very recently, P, PI and PID conventional controllers were used [39], [40], [41]for WECS control. Such regulators do not maximize efficiency, while limiting mechanical fatigue of the system. Therefore, it is crucial to use robust controllers in wind industry.

Among the different existing methods, variable gain controllers were proposed in [42] and [43]while using linear models with varying parameters (LPV) [44]. Unfortunately, this control strategy presents low efficiency since it does not limit the mechanical fatigue of the system. Adaptive algorithm [45] predictive control [46] fuzzy logic approaches [47] and predictive control using linear matrix inequalities (LMI) [48] were proposed for the MPPT control. In the mentioned works, the regulation strategy was tested in the second zone or the full load zone where the power extracted by the wind turbine must be limited. Some studies have also compared the linear against non-linear control strategies [49]. The good performance of H_∞regulators in controlling WECS was demonstrated in numerous researches [50]. A comparison between the LQG and the H_∞ regulators [51], showed that the two controllers had the same effectiveness in terms of energy production. A comparative study, conducted in [50], proved that H_∞ regulator is more performant that the conventional PID controllers. In addition, the CRONE controller is widely used for vehicles (braking system [52], pneumatic suspension system [53]). Indeed, few references deal with the CRONE control strategy in the WECS domain and the focus has been on zone II as in [54], [55], and [56]. As far as we know, we are the first to propose the use of a Fractional Order PI controller for speed regulation in a WECS based on DESG.

IV. ANALYTICAL SIZING OF A DESG 1.5 MW

To size a generator for the 1.5 MW turbine, two methods can be considered: the use of a multi-physics behavioral model or a dimensioning analytical model. The first method is more cumbersome to use because it requires the physical description of the model and it must be associated with optimization algorithms. The second method is simpler to implement and faster. Our goal is to obtain an order of magnitude of the electrical parameters of a DESG of 1.5 MW to the amount of implementing an appropriate control technique. So, the 2nd method is sufficient for the sizing of our generator.

The so-called ''analytical'' method entails calculating the geometric parameters of an HG based on certain basic specifications (base speed, voltage, ...). We begin by creating specifications in order to discover all of the machines that meet them. These generators have to produce the desired base torque at the selected base speed. The next step consists of calculating permeances and fluxes. It is presumed that the DESC is a Park one in this case [19].

A. SPECIFICATIONS

To size the 1.5 MW hybrid generator, it is necessary to set a number of parameters according to which, we will then calculate the electrical quantities of the generator. φ_{ext}, p, the salience ratio s_s and the hybridization ratio α' are kept the same as the SATIE laboratory prototype (1). It should be noted that this prototype is a 3kW machine, with 6 pole pairs, the maximum excitation current I_{ema} is about 8A and the stator nominal current is equal to 10A.

$$\begin{cases} \varphi_{ext} = \phi_{a-3kW} + M_{3kW} \cdot I_{e\max-3kW} = 0,071\text{wb} \\ s_s = L_{q-3kW} / L_{d-3kW} = 1,7736 \\ \alpha' = \phi_{a-3kW} / \phi_{ext-3kW} = 0,53 \end{cases} \quad (1)$$

$\varphi_{ext-3kW}$	3kW HG total excitation flux
Φ_{a-3kW}	3kW HG flux created by the PMs
M_{3kW}	3kW HG mutual inductance
L_{q-3kW}	3kW HG inductance on the q-axis
L_{d-3kW}	3kW HG inductance on the d-axis
$I_{emax-3kW}$	3kW HG maximum excitation current

The following specifications are fixed for designing the 1.5MW HG [18], [57]:

Ω_b	base speed (rd/s)	188.5
n_s	number of turns	10
P_D^*	d-axis normalized permeance	0.3
η	Yield	0.95
σ	Blondel coefficient	0.4
V_{sb}	basic stator voltage	690V

B. SIZING APPROCH

In this section, we provide a detailed description of the three steps required for the design of synchronous magnet machines in our approach. Starting from an infinite number of machines (meeting the specifications we set or not), the first part consists of determining the set of machines that meet the electromagnetic specifications. This involves finding machines capable of providing the base torque C_{emb} at the base speed ω_b. This step allows for the transition from electromagnetic specification data to the geometric dimensions of the considered machine. It is divided into two parts. The first part involves the calculation of permeances and flux in vacuum (i.e., magnetic parameters) from the electromagnetic specification data. We refer to this data as input data, while the magnetic parameters will be intermediate data. In the design process, this step is particularly interesting as it is seen to be generic. The only assumption made here is that the synchronous machine under study is a Park machine (which nevertheless remains a rather strong assumption). Thus, this module is usable regardless of the type of Park synchronous machine one wishes to model. Additionally, it will be observed that regardless of the model used, the inversion of this system is always analytical. As a result, the intermediate data of this model always strictly adhere to the equality constraints imposed by the input data on the one hand and the computation time is minimized on the other hand. The second part will allow us to obtain the dimensions of the machine (referred to as output data) from the previously determined magnetic parameters. We will obtain these output data using models based on reluctance networks. Here, the dimensions of the machine are determined based on the magnetic data (permeances and flux in vacuum) calculated in the first part. In this phase, it is clear that the modeling will depend on the machine under study. The analytical calculation of the electrical parameters of a DESG is detailed in [19]. This paragraph summarizes the main steps for estimating these parameters:

1. Calculation of the basic torque such as:

$$C_b = \mathrm{P_b}/\Omega_\mathrm{b} \tag{2}$$

2. Determination of the voltage of the coil(V):

$$v_{sb} = V_{sb}/n_s \tag{3}$$

3. Basic pulse calculation (rd/s):

$$w_b = p \cdot \Omega_b \tag{4}$$

4. Determination of the optimal load angle ψ_{bopt} between the current and the electromagnetic force of the same stator phase at the base point as follows:
The proportionality coefficient is defined in the case of the no-loss model noted ς_b (5).

$$\varsigma_b = \cos\psi_{\mathrm{bopt}} + 0.5 \times \mathrm{P}^*_D(1\text{-}\mathrm{s}_s) \cdot \sin 2\psi_{\mathrm{bopt}} \tag{5}$$

In generator operation, the optimal load angle ψ_{bopt} minimizes ς_b. $(d\varsigma_b/d\psi_{\mathrm{bopt}} = 0)$

$$\begin{cases} \dfrac{d\varsigma_b}{d\psi_{\mathrm{bopt}}} = -\sin\psi_{\mathrm{bopt}} + \mathrm{P}^*_\mathrm{D} \cdot (1-\mathrm{s}_s) \cdot \cos 2\psi_{\mathrm{bopt}} \\ = -\sin\psi_{\mathrm{bopt}} + \mathrm{P}^*_\mathrm{D} \cdot (1-\mathrm{s}_s) \cdot \left(1 - 2\sin\psi^2_{\mathrm{bopt}}\right) \\ = -\sin\psi_{\mathrm{bopt}} - 2 \cdot \mathrm{P}^+_\mathrm{D} \cdot (1-\mathrm{s}_s) \cdot \sin\psi^2_{\mathrm{bopt}} \\ \quad + \mathrm{P}^*_D \cdot (1-\mathrm{s}_s) \end{cases}$$

$$\rightarrow \begin{cases} \Delta = 1 + 8\mathrm{P}^{*2}_D\,(1-\mathrm{s}_s)^2 \\ \sin\psi_{\mathrm{bopt1}} = \dfrac{1-\sqrt{\Delta}}{-4\mathrm{P}^*_\mathrm{D}\,(1-\mathrm{s}_s)} \\ \quad = -0.289 \text{ (selected solution)} \\ \sin\psi_{\mathrm{bopt2}} = \dfrac{1+\sqrt{\Delta}}{-4\mathrm{P}^*_\mathrm{D}\,(1-\mathrm{s}_s)} \\ \quad = 2.289 \text{ (indeterminate form)} \end{cases}$$

This involves:

$$\begin{aligned} \psi_{\text{bopt-}\alpha} &= \sin^{-1}(-0.289) = -0.29 \\ \pi - \psi_{\text{bopt-}\beta} &= \sin^{-1}(-0.289) = -0.92 \end{aligned} \tag{6}$$

Combining (5) and (6) involves:

$$\begin{aligned} \zeta_{b_a}(\psi_{\text{bopt-}\alpha}) &= 0.99(\text{engine} - \text{operation}) \\ \zeta_{b_b}(\psi_{\text{bopt-}\beta}) &= -0.92(\text{retained solution}) \end{aligned} \tag{7}$$

5. Flux φ_{exc} per whorl (Wb):

$$\varphi_{exc} = v_{sb}/w_b \cdot \gamma_b \tag{8}$$

where is defined by: γ_b

$$\begin{aligned} \gamma_b^2 = &\left(\mathrm{r}^*_\mathrm{s} \cdot \sin\psi_{\mathrm{bopt}}\text{-}\mathrm{s}_s \cdot \mathrm{P}^*_D \cdot \cos\psi_{\mathrm{bopt}}\right)^2 \\ &+ \left(\mathrm{r}^*_\mathrm{s} \cdot \cos\psi_{\mathrm{bopt}} + \mathrm{P}^*_D \cdot \sin\psi_{\mathrm{bopt}} + 1\right)^2 \end{aligned} \tag{9}$$

6. Magnetomotrice Force A_s (At):

$$A_s = C_b/3 \cdot p \cdot \varphi_{exc} \cdot \varsigma_{bopt} \tag{10}$$

7. Specific standardized resistance modeling Joule losses:

$$r^*_s = r_s A_s/\phi_{exc}\omega_b \tag{11}$$

8. Permeance (H):

$$P_D = P^*_D \cdot \varphi_{exc}/A_{sb} \quad P_Q = \mathrm{s}_s \cdot P_D \tag{12}$$

9. Inductance (H):

$$L_d = n_s^2 \cdot P_D \quad L_q = n_s^2 \cdot P_Q \tag{13}$$

10. Specific resistance (Ω):

$$r_s = r^*_s \cdot \varphi_{exc}/A_{sb} \tag{14}$$

11. Stator resistance (Ω):

$$R_s = n_s^2 \cdot r_s \tag{15}$$

12. Flux of magnets (Wb):

$$\phi_a = \alpha' \cdot \varphi_{exc} \cdot n \tag{16}$$

TABLE 1. 1.5 MW DESG electrical parameter.

Symbol	Quantity
P_n (kW)	1500
p	6
Φa(Wb)	0.25
Ld (mH)	0.14
Lq (mH)	0.2
Le (mH)	176
Rs (Ω)	0.024
Re (Ω)	0.7
Me (mH)	2.2

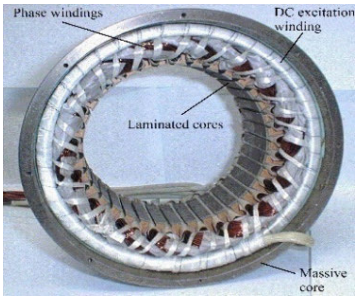

(a) Stator

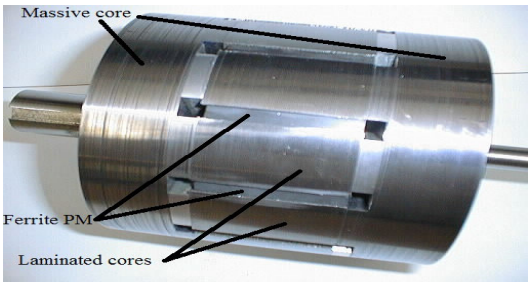

(b) Rotor

FIGURE 7. Topology studied.

13. Mutual inductance:

$$M = \varphi_{exc} \cdot n - \phi_a / I_{e\max} \tag{17}$$

With I_{emax} the 1.5 MW HG maximum excitation current is equal to 100A [18]

14. Excitation inductance and resistance:

$$L_e = 3M^2 / L_d \cdot (1-\sigma) R_e = V_e / I_{e\max} \tag{18}$$

where V_e =70V is DC/DC convertor supply voltage of the chopper.

The solution of these equations makes it possible to deduce the electrical parameters of the generator defined in the following table:

V. MODELLING OF THE DESG STUDIED STRUCTURE

The machine employed is a synchronous flux concentration machine with the EC at the stator and PMs buried in the rotor (FIGURE 7). The stator is built with massive and laminated cores. Magnetic collectors are used to connect the magnetic circuits of the stator and rotor. The EF collected in the air gap is thus generated by two sources: a constant amplitude flux from the magnets buried at the rotor with ortho-radial magnetization, and an adjustable flux generated by the wound excitation placed at the stator.

The equations that govern the operation of the DESG in the reference frame (a,b,c) are given by system (19) [24].

Flux

$$\phi_e = [M_{3e}]^t [I_3] + L_e I_e + \phi_{ae}$$
$$[\phi_3] = [L_3][I_3] + [M_{3e}] I_e + [\phi_{3e}]$$

Voltages

$$V_e = R_e I_e + d\phi_e / dt$$
$$[V_3] = R_s [I_3] + d[\phi_3] / dt \tag{19}$$

Electro-magnetic torque

$$C_{em} = \frac{1}{2} [I_3]^t \frac{d[L_3]}{d\theta} [I_3] + [I_3]^t \frac{d[M_{3e}]}{d\theta} [I_3] + [I_3]^t \frac{d[\phi_{3e}]}{d\theta}$$

With

$[\phi_3]^t = [\phi_a \phi_b \phi_c]$
Stator flux vector

$[I_3]^t = [I_a I_b I_c]$
Statorcurrentvector

$[V_3]^t = [V_a V_b V_c]$
Stator voltage vector

$[\phi_{e3}]^t = [\phi_{ea} \phi_{eb} \phi_{ec}]$
EF produced b yPMin statorcoils

$[M_{e3}]^t = [M_{ea} M_{eb} M_{ec}]$
Vector of stator − excitation mutual

$$[L_3] = \begin{bmatrix} l_{aa} & m_{ab} & m_{ac} \\ m_{ab} & l_{bb} & m_{bc} \\ m_{ac} & m_{bc} & l_{cc} \end{bmatrix}$$
Stator inductor matrix

R_s
Armature resistance

V_e, L_e and R_e
Excitation voltage, coil inductance and coil resistance

A. FIRST HARMONIC MODEL

In the first harmonic hypothesis, the matrices $[L_3]$, $[M_{e3}]$ and $[\varphi_{e3}]$ can be expressed as [18] and [24] (20)–(22), as shown at the bottom of the next page, where M_0 is the maximum mutual inductance between the inductor and the armature and ϕ_a is the maximum flux created by the PM. Here, it is assumed that all quantities are perfectly sinusoidal. The equations of the DESG in Park's reference frame are given by: [18] and [19].

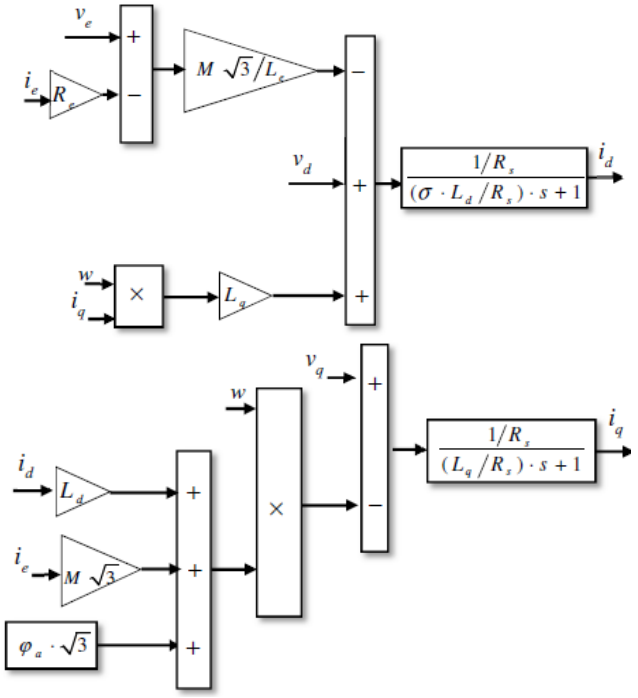

FIGURE 8. Block diagram of the current on the 'd' and 'q' axis.

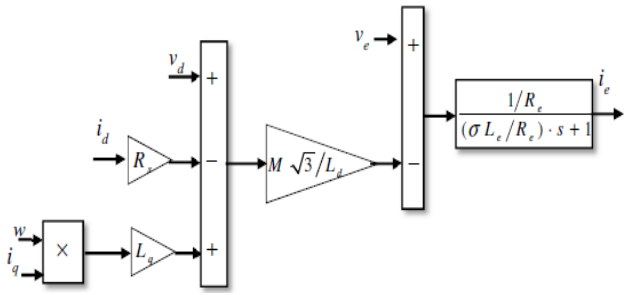

FIGURE 9. Block diagram of the excitation current.

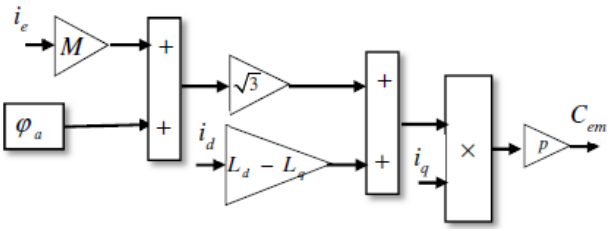

FIGURE 10. Block diagram of the electromagnetic torque.

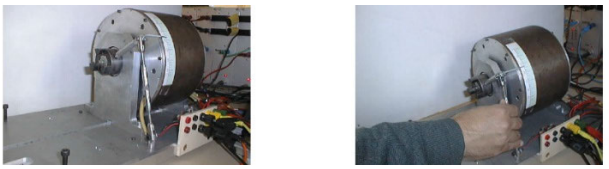

FIGURE 11. Measurement of inductances.

Voltages

$$\begin{cases} v_d = R_s i_d + \dfrac{d\varphi_d}{dt} - \Omega_g \varphi_q \\ v_q = R_s i_q + \dfrac{d\varphi_q}{dt} + \Omega_g \varphi_d \\ v_e = R_e i_e + \dfrac{d\varphi_e}{dt} \end{cases} \tag{23}$$

Flux

$$\begin{cases} \varphi_d = L_d i_d + M\sqrt{3}\, i_e + \varphi_a\sqrt{3} \\ \varphi_q = L_q i_q \\ \varphi_e = M\sqrt{3}\, i_d + L_e i_e + \varphi_{ae} \end{cases}$$

Electro-magnetic torque

$$C_{em} = p \times i_q \times \left[\sqrt{3} \times (\varphi_a + M \cdot i_e) + (L_d - L_q) \cdot i_d\right]$$

Where v_d, v_q and v_e are respectively the voltages on the d and q axes and the DC voltage of the EC, i_d, i_q are the currents on the d and q axes, respectively. φ_d, φ_q and φ_e are the flows on the d and q axes and the EC respectively. L_d, L_q and M are respectively the inductance on the axes d and q and the mutual inductance. φ_a is the flux created by the magnets on a stator winding and φ_{ae} is the PM's flux created on an excitation winding.

A "motor" convention is applied for the modeling of the DESG, a negative torque is then derived from our model. In this modeling mode, the inputs of our model are the voltages and the outputs are the currents. Using system (23) block diagrams representing the models of direct, the quadrature current, the excitation current and the electromagnetic torque can be established. They are given in the following figures.

w is the electric pulse and σ is the Blondel coefficient are defined in (24) [18]

$$w = p \cdot \Omega_g \quad \sigma = 1 - 3M^2 \Big/ L_d L_e \tag{24}$$

B. GENERATOR MODELING TAKING INTO ACCOUNT SPACE HARMONICS

As we do not dispose of a real 1.5MW DESG, the 3kw small prototype is used to approximate a mathematical model of

$$[L_3] = \begin{bmatrix} L_{s0} & M_s & M_s \\ M_s & L_{s0} & M_s \\ M_s & M_s & L_{s0} \end{bmatrix} + L_{s2} \begin{bmatrix} \cos(2p\theta) & \cos(2p\theta - 2\pi/3) & \cos(2p\theta - 4\pi/3) \\ \cos(2p\theta - 2\pi/3) & \cos(2p\theta - 4\pi/3) & \cos(2p\theta) \\ \cos(2p\theta - 4\pi/3) & \cos(2p\theta) & \cos(2p\theta - 2\pi/3) \end{bmatrix} \tag{20}$$

$$[M_{e3}] = M_0 \begin{bmatrix} \cos(2p\theta) & \cos(2p\theta - 2\pi/3) & \cos(2p\theta - 4\pi/3) \end{bmatrix} \tag{21}$$

$$[\phi_{e3}] = \phi_a \cdot \begin{bmatrix} \cos(2p\theta) & \cos(2p\theta - 2\pi/3) & \cos(2p\theta - 4\pi/3) \end{bmatrix} \tag{22}$$

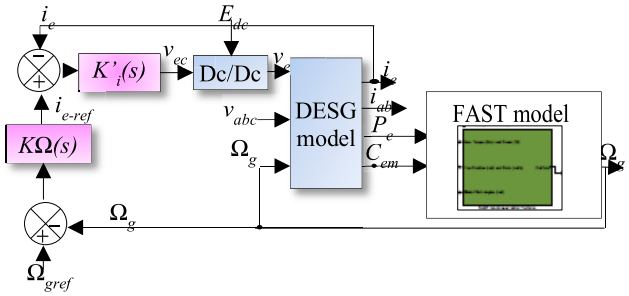

FIGURE 12. The WCS bloc diagram.

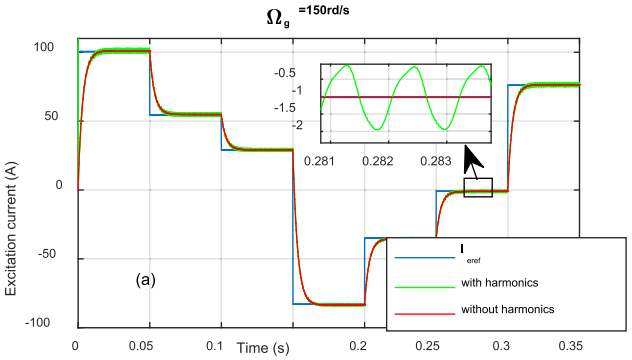

FIGURE 13. current loop response regarding space harmonics.

a parallel structure DESG tacking into account space harmonic effects. A 50Hz sinusoidal voltage and an adjustable amplitude power a stator winding (FIGURE 11). The DESG's detent torque is sufficient to hold it stationary. The voltammetric approach is then used to determine L_d, L_q and M.

Finally, the approximative mathematic model is obtained by an FFT analysis (25) [24]

$$\begin{cases} L = L_d + L_q/3 + \sum_{j=1}^{9} L_{s_{2j}} cos(2jp\theta - \zeta_j) \\ M = -L_d - L_q/3 + \sum_{j=1}^{9} M_{s_{2j}} cos(2jp\theta - \zeta_j) \\ \phi_e = \sum_{j=0}^{8} \phi_{a_{(2j+1)}} cos(p\theta(2j+1) - \zeta_j) \end{cases} \quad (25)$$

The DESG model is finally defined in the Concordia coordinate system (26)([24].

Flux

$$[\phi_2] = [L_2][I_2] + [M_{e2}]I_e + [\phi_{e2}]$$
$$\phi_e = [M_{e2}]^t[I_2] + L_e I_e + \phi_{ae}$$

Voltages

$$V_e = R_e I_e + d\phi_e/dt$$
$$[V_3] = R_s[I_3] + d[\phi_3]/dt \quad (26)$$

Electro-magnetic torque

$$C_{em} = \frac{1}{2}[I_2]^t \frac{d[L_2]}{d\theta}[I_2] + [I_2]^t \frac{d[M_{2e}]}{d\theta}[I_2] + [I_2]^t \frac{d[\phi_{2e}]}{d\theta}$$
$$[I_2]^t = \begin{bmatrix} I_\alpha I_\beta \end{bmatrix} \ [\phi_2]^t = \begin{bmatrix} \phi_\alpha \phi_\beta \end{bmatrix} \ [M_{e2}]^t = \begin{bmatrix} M_{e\alpha} M_{e\beta} \end{bmatrix}$$
$$[V_2]^t = \begin{bmatrix} V_\alpha V_\beta \end{bmatrix} \ [\phi_{e2}]^t = \begin{bmatrix} \phi_{e\alpha} \phi_{e\beta} \end{bmatrix} \ [L_2] = \begin{bmatrix} L_\alpha & M_{\alpha\beta} \\ M_{\alpha\beta} & L_\beta \end{bmatrix}$$

VI. ELECTRICAL CONTROL OF THE WIND SYSTEM

The 1.5MW turbine is electrically controlled by two loops; the internal one is the excitation current and the outer loop is the velocity.

The system frame work is in FIGURE 12

The complete mechanical and aerodynamic models are implemented, under the professional simulator FAST [16] using the WindPACT (WP) turbine.

The NREL (National Renewable Energy Laboratory) sponsored the development, verification, and validation of various computer-assisted engineering tools for predicting the loads and responses of wind turbines. The FAST code was developed through a subcontract between NREL and Oregon State University. FAST is a comprehensive aeroelastic simulator that allows for simulating and studying wind turbine behavior under various conditions. In particular, it predicts extreme loads and fatigue of horizontal-axis wind turbines with two or three blades.

During the time domain analysis, FAST allows controlling the model at different levels. Five controls are available: blade pitching, generator torque control, applying the fast shaft brake, deploying blade tip brakes, and yawing the nacelle. The simplest turbine control methods only require defining certain parameters in the main parameter file. More complicated control methods (such as ours) require writing specific routines, compiling them, and linking them to the rest of the program. An interface between FAST and Simulink is available (FIGURE 12). It allows for implementing turbine controls from functional diagrams. To do this, FAST subroutines are linked to a Matlab/Simulink "S-Function" and use the equations describing the mechanical and aerodynamic behavior of the turbine available in FAST in this environment. This introduces great flexibility in wind turbine control implementation. The generator torque, nacelle, and pitch angle control modules can be designed in the Simulink environment and simulated using the complete motion equations describing the aeroelastic phenomena of a wind turbine available in FAST. The wind turbine block, as illustrated in FIGURE 12, contains the S-Function block with mechanical and aerodynamic equations. It also contains blocks that integrate accelerations to obtain velocities and displacements. Thus, the motion equations are formulated in the FAST "S-Function" but solved using one of the Simulink solvers. The FAST model is then linked to our advanced DESG model.

A. CURRENT LOOP

1) CALCULATION OF THE CURRENT REGULATOR

The current loop model can be approximated by a first order (27) [56] and a simple PI is sufficient for control. The

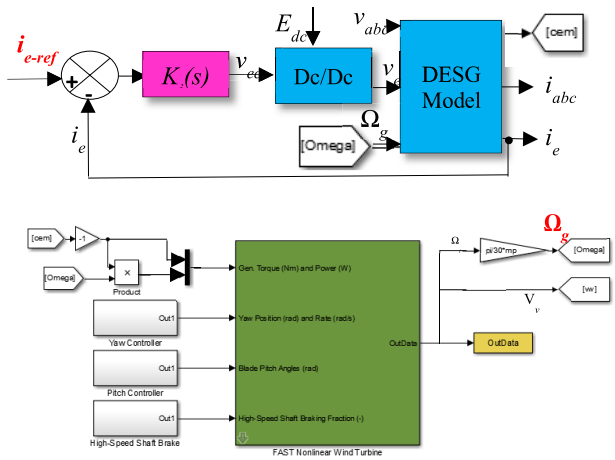

FIGURE 14. WCS linearization method.

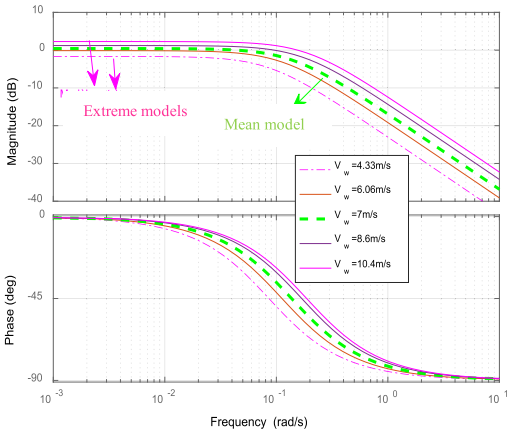

FIGURE 15. Bode diagram of Ωg(s)/ieref(s) for various operating points.

settling time is 10ms and the bandwidth is 310rd/s [57].

$$\frac{v_{ec}(s)}{i_e(s)} = \frac{G_0/R_e}{1+\sigma L_e/R_e} \tag{27}$$

Here, G_0=*10* is the chopper's gain. The current corrector is given by (28).

$$K_i(s) = K_i\frac{\sigma L_e/R_e \cdot s+1}{\sigma L_e/R_e \cdot s} = 3.52\frac{0.1s+1}{0.1s} \tag{28}$$

2) CURRENT CORRECTOR VALIDATION

The current regulator is designed based on the Park model (the harmonics are not considered while calculating the excitation current controller).

FIGURE 13 shows that the regulator guarantees a good reference tracking and a response time not exceeding 10ms. Oscillations of about 1 A (1% with respect to I_{emax}) are observed.

B. SPEED LOOP

A Fractional order PI controller is considered in this work.

1) LINEARIZATION

Given the non-linearity of the relation Ω_g=$f(i_e)$, an experimental identification conducted under the FAST simulator for 5 wind speeds values in zone II is performed.

An equivalent linear model is derived by analyzing the output Ω_g in terms of overshoot and settling time for a specific input signal ieref, which corresponds to an operational point.

Zone 2 contains wind speeds ranging from 3m/s to 11m/s; in this zone, the ideal turbine rotation speed (or generator rotation speed) is a linear function. As a result, four operational sites are chosen that are evenly dispersed over zone 2: the wind speeds are set to 4.33, 6.06, 7, 8.6 and 10.4 m/s, respectively. After obtaining a collection of transfer functions from the input (i_{eref}) to the output (Ω_g), an average model is picked.

The linearized model is obtained through simulations conducted on the full Simulink model of the WCS (FIGURE 14), where switching effects, spatial harmonics, and transmission shaft flexibilities are accounted.

The Bode diagram of these transfer functions is shown in FIGURE 15.

An average plant model is approximated by a transfer function describing the behavior of the WECS (29).

$$G(s) = \frac{\Omega_g(s)}{i_{eref}(s)} = \frac{1.1}{7.66s+1} \tag{29}$$

2) CALCULATION OF SPEED CONTROLLER

The regulator is calculated for the following specifications:

- A zero-static error in steady state.
- A bandwidth around 2rd/s: this value of the bandwidth allows to have a fast-enough speed loop response.

The goal of the design is to tune the $PI^{\lambda}D^{\mu}$ (30)controller's parameters (K_c, T_I, TD, λ and μ) so that the closed loop TF $G_A(s)$ (31) ≈G_d(s) (32) in a specified frequency range centered $\omega_c = \omega_u$ [58].

$$C(s) = K_c + \frac{T_I}{s^{\lambda}} + T_D s^{\mu} \tag{30}$$

$$G_A(s) = \frac{Y(s)}{R(s)} = \frac{C(s)H(s)}{1+C(s)H(s)} \tag{31}$$

$$G_d(s) = 1\Big/1+\left(\frac{s}{\omega_u}\right)^m \tag{32}$$

The controller is calibrated to enforce the process output's reaction to the desired setpoint while maintaining system stability. The issue arises in determining the proper C(s) controller to guarantee that the closed-loop TF G_A(s) act like the specified reference model. Gd(s) is defined as: G_d (s) (32).

G_d (s) is a mathematical equation with a positive real integer, ω_u, with m values from 0 to 2. If m is between 0 and 1, the equation becomes a relaxation system; if m is between 1 and 2, the equation becomes an oscillating system.

To meet desired performance requirements for phase margin (φ_m), crossover frequency (ω_c), and unity gain (ω_u),

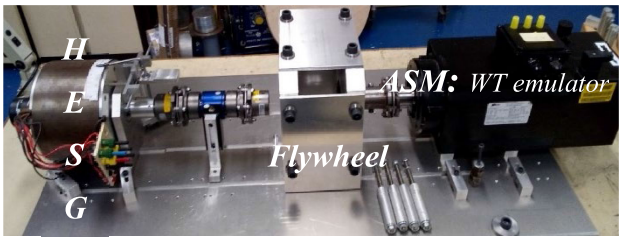

FIGURE 16. Experimental 3kW test bench.

the parameters m and ω_u can be determined as follows: ω_u corresponds to the unity gain at the desired ω_c, where ω_c is the unity gain crossover frequency of the projected feedback control system. Setting ω_u correctly allows the system to run efficiently, maintain stability, and satisfy performance requirements.

m represents the intended φ_m and may be computed as $m = 2[1-(\varphi_m/\pi)]$, where φ_m is the phase margin of the proposed feedback control system. This allows the system to attain the appropriate degree of performance and stability.

The FOPI regulator is computed with the MATLAB FOMCON toolbox:

$$G_d(s) = \frac{1}{1+\left(\frac{s}{\omega_u}\right)^m} = \frac{1}{1+\left(\frac{s}{7.66}\right)^{1.05}} \tag{33}$$

$$y(t) = L^{-1}\left\{\frac{1}{s}\left[\frac{1}{1+\left(\frac{s}{7.66}\right)^{1.05}}\right]\right\} = 1 - E_{1.05}\left[-(7.66t)^{1.05}\right] \tag{34}$$

VII. SIMULATION RESULTS

The proposed approach is validated experimentally in previous works [59], [60]on a test bench of a 3kW DESG based WCS where the wind turbine is replaced with an asynchronous servo-motor (FIGURE 16). In these works, a CRONE and an H_∞ regulator are compared and the performance of the CRONE controller is proved. In addition, [60], compared the performance of the FOPI versus the CRONE regulator in turms of optimal generator speed tracking. It turns out that the FOPI controller outperform the previously tested one.

Establishing an experimental test bench for a large-scale wind conversion system (WCS) can be difficult because to the cost, size, and complexity of the electrical and mechanical components, particularly in an academic research setting. As a result, the purpose of this work is to provide an alternative through the creation of a realistic simulation model. Such a model is required for a more accurate performance evaluation of the researched 1.5 MW aerogenerator, which is based on a Hybrid Excitation Synchronous Generator (DESG). The code FAST is used to create a WCS model that accounts for both complicated electrical events and aerodynamic dynamics.

In this work, spatial harmonics are considered. The purpose is to assess the effectiveness of speed corrector from the point

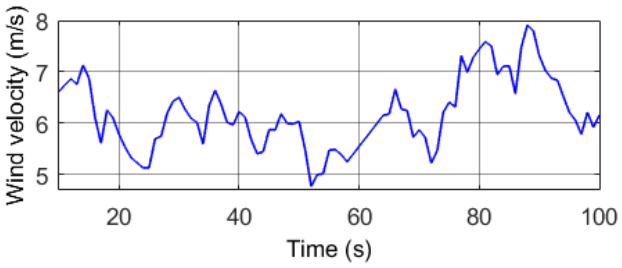

FIGURE 17. Wind speed as a function of time.

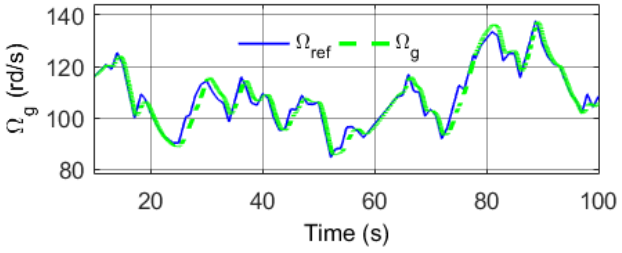

FIGURE 18. Rotational speed as a function of time.

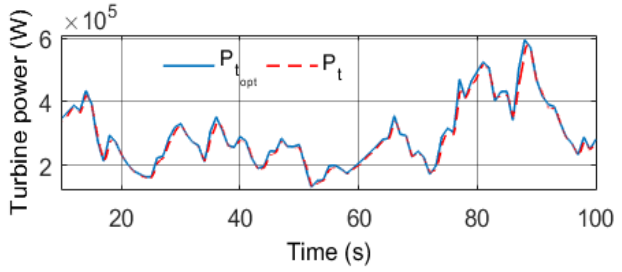

FIGURE 19. Turbine power as a function of time.

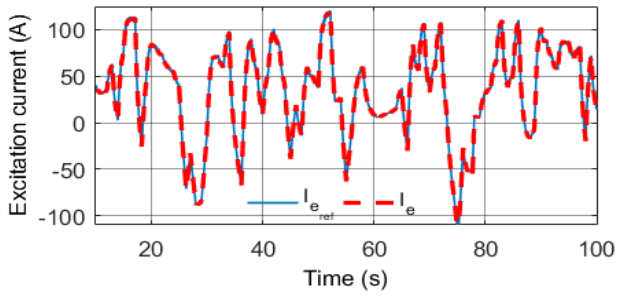

FIGURE 20. Excitation current as a function of time.

of view of reference monitoring and vibration minimization on the fast shaft side. This test is conducted under a realistic wind profile (FIGURE 17) and for an average wind speed of 6.5 m/s.

In zone II, the effects of structural loads are minimal. The purpose of the control in this area is to maximize the power extracted from the wind by ensuring a good follow-up of the rotational speed. This is verified in our case (FIGURE 18). The comparison of the aerodynamic power extracted from the wind with the maximum recoverable power (FIGURE 19), given by equation (35) [61], shows that optimal extraction

of power is ensured at all times without the control current saturating (I_{emax} is about 100 A): the current used to cancel the error between the reference and the actual speed is adequate (FIGURE 20). This validates that the bandwidth chosen (and thus the fixed response time) for the speed corrector setting ensures a compromise between speed, stability and accuracy and it is suitable for a wind turbine.

$$P_{t_{opt}} = 0.5 \cdot C_{p_{opt}} \cdot \rho \cdot S \cdot V_w^3 \; Where \; C_{p_{opt}} = 0.5 \; [63] \quad (35)$$

Van der Hoven's spectral model is now used to simulate the wind data, and the TurbSim program is used to introduce turbulence using the Kaimal spectrum (FIGURE 21), a noteworthy accomplishment with important implications for mechanical stability is the effective velocity tracking shown in the complete load zone of the wind conversion system (WECS) simulation carried out under the Fatigue Aerodynamic Structure and Turbulence (FAST) framework (FIGURE 22). This result is extremely important for a number of reasons.

First off, the WCS exhibits efficient load management and balancing in its mechanical components, including the rotor, gearbox, and generator, by functioning within the ideal power output range. This reduces mechanical stress and lowers the risk of fatigue-related failures, which increases system lifetime and dependability.

Second, the precise velocity monitoring performed across the load zone confirms that the speed regulators are functioning properly, adjusting the generator speed and torque to fit the prevailing wind conditions. This capacity to maintain constant rotational speed and torque lowers vibration and oscillations, preventing potential resonance-induced damage and improving mechanical integrity throughout the WCS.

Furthermore, the WCS's ability to respond swiftly to changes in wind speed and monitor the desired velocity throughout the whole load zone proves its dynamic reaction capabilities [63]. This quick responsiveness contributes to the system's dependable mechanical operation by allowing for smoother and more predictable pressures on mechanical components. Such stability is essential for the WCS's overall mechanical health, minimizing wear and tear, and enhancing performance.

The slow shaft torque over time in a wind conversion system model is displayed in Fig 18 and is an important signal for evaluating the efficiency of speed regulators. The torque generated by the wind turbine rotor corresponds to the slow shaft torque employed in wind conversion systems. The speed regulators adjust the generator speed and torque to optimal power production. By examining the slow shaft torque, this graph allows for a detailed evaluation of the speed regulators' performance in system control. The graph's time axis gives light on the regulators' dynamic behavior and shows how sensitive they are to changes in wind conditions. Smooth torque fluctuations indicate efficient power output and little mechanical stress. The speed regulators may have problems, such as insufficient control algorithms, mechanical problems, or poor sensor feedback, if they deviate from the planned

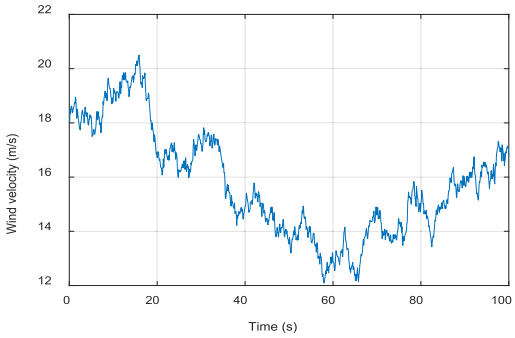

FIGURE 21. Wind speed as a function of time.

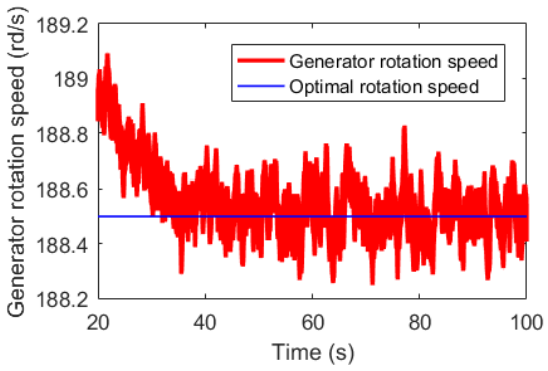

FIGURE 22. Rotational speed as a function of time.

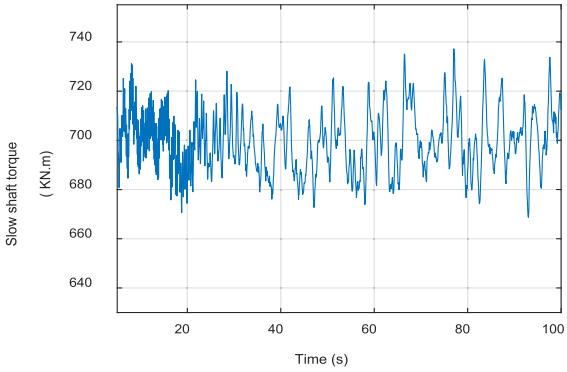

FIGURE 23. Slow shaft torque as a function of time.

behavior. As a result, FIGURE 23 is a useful diagnostic tool for assessing how well speed regulators in wind conversion systems are working.

Compared to the results presented in [62] a considerable minimization in the slow shaft vibration is obtained (150kN.m in [62]versus 50kN.m in the present work). It should be noted that the authors of [62] used an antiwindup gain scheduled PID controller for the WP turbine [16].

VIII. CONCLUSION

This article has introduced the general framework of our team research work. In the first part, an overview of the technology of hybrid excitation machines was presented and a classification was given considering a series or parallel structure. A state of the art of the different uses of this generator is also presented. The article provides a thorough description of

DESGs and presents a mathematical model based on experimental investigation of a 3kW laboratory prototype, allowing for accurate representation of space harmonics. The precise mathematical model of the DESG, which can be used as a reference for future research, is one of the study's significant achievements.

In addition, the research provides an analytical method for DESG sizing and analyzes the performance FOPI controller on a 1.5MW wind conversion system. The findings of this study give useful information on the performance of the speed regulator in the wind conversion system. The speed regulator maximizes power generation and maintains stable operation within the intended operational range by utilizing effective load management and accurate regulation of generator speed and torque. The study of different performance indicators, including as power production, pitch angle control, and rotor speed stability, demonstrates the speed regulator's usefulness in optimizing the WCS's performance.

Finally, a notable result in this study is the significant reduction in slow shaft vibration as compared to previously unpublicized work in the WP turbine. The sluggish shaft vibration was previously reported to be 150 kNm, however the current experiment got a substantially lower value of 50 kNm. These findings highlight the enhanced mechanical stability produced by optimizing the speed regulator's performance. The reduction in slow shaft vibration suggests less mechanical stress on the system, lowering the chance of fatigue-related failures and extending the WCES's life.

Future research will center on connecting the 1.5MW turbine model with a DESG into the grid to investigate issues like as grid stability and power quality. Researchers will investigate a variety of grid integration methodologies, including enhanced forecasting algorithms, optimum scheduling, and grid-friendly operating strategies. Furthermore, there will be a sustained emphasis on developing grid connection technologies and combining energy storage systems with wind farms to reduce unpredictability and intermittency, providing a consistent and sustainable electricity supply.

AUTHOR CONTRIBUTIONS

The work presented here was a cooperative effort by all the authors.

CONFLICTS OF INTEREST

The authors declare no conflict of interest.

DATA AVAILABILITY STATEMENT

The authors confirm that the data supporting the findings of this study are available within the article.

ACKNOWLEDGMENT

The authors extend their appreciation to King Saud University in Riyadh, Saudi Arabia for funding this research work through researchers supporting project number (RSPD2024R683).

REFERENCES

[1] R. Özkan and M. S. Genç, "Aerodynamic design and optimization of a small-scale wind turbine blade using a novel artificial bee colony algorithm based on blade element momentum (ABC-BEM) theory," *Energy Convers. Manage.*, vol. 283, May 2023, Art. no. 116937.

[2] A. M. Shawqran, A. El-Marhomy, M. A. Attia, A. Y. Abdelaziz, and H. H. Alhelou, "Enhancement of wind energy conversion system performance using adaptive fractional order PI blade angle controller," *Heliyon*, vol. 7, no. 10, Oct. 2021, Art. no. e08239.

[3] P. D. Clausen, S. P. Evans, and D. H. Wood, "Design, manufacture, and testing of small wind turbine blades," in *Advances in Wind Turbine Blade Design and Materials*. Univ. of Newcastle, 2023, pp. 441–461.

[4] L. Pontes, T. Costa, A. Souza, N. Dantas, A. Vasconcelos, G. Rissi, R. Dias, M. A. Mohamed, P. Siano, and M. Marinho, "Operational data analysis of a battery energy storage system to support wind energy generation," *Energies*, vol. 16, no. 3, p. 1468, Feb. 2023.

[5] M. Adib, F. Nasiri, and F. Haghighat, "Integrating wind energy and compressed air energy storage for remote communities: A bi-level programming approach," *J. Energy Storage*, vol. 72, Nov. 2023, Art. no. 108496.

[6] E. C. Edwards, A. Holcombe, S. Brown, E. Ransley, M. Hann, and D. Greaves, "Evolution of floating offshore wind platforms: A review of at-sea devices," *Renew. Sustain. Energy Rev.*, vol. 183, Sep. 2023, Art. no. 113416.

[7] A. Loulijat, H. Chojaa, M. El Marghichi, N. Ettalabi, A. Hilali, A. B. Barnawi, Z. M. S. Elbarbary, and M. A. Mossa, "Application and comparison of a modified protection scheme utilizing a proportional–integral controller with a conventional design to enhance doubly fed induction generator wind farm operations during a balanced voltage dip," *Processes*, vol. 11, no. 10, p. 2834, Sep. 2023.

[8] S. Puchalapalli, B. Singh, and S. Das, "Synchronizing control of wind turbine driven doubly fed induction generator system with DG in remote area involving solar PV-battery energy storage," *IEEE Trans. Ind. Appl.*, 2023.

[9] M. A. Mostafa, E. A. El-Hay, and M. M. El-Kholy, "Optimal maximum power point tracking of wind turbine doubly fed induction generator based on driving training algorithm," *Wind Eng.*, vol. 47, no. 3, pp. 671–687, Jun. 2023.

[10] A. Rahman, R. Dutta, G. Chu, D. Xiao, V. K. Thippiripati, and M. F. Rahman, "Open-winding permanent magnet synchronous generator for renewable energy—A review," *Energies*, vol. 16, no. 14, p. 5268, Jul. 2023.

[11] S. A. Ashrafzadeh, A. A. Ghadimi, A. Jabbari, and M. R. Miveh, "Optimal design of a modular axial-flux permanent-magnet synchronous generator for gearless wind turbine applications," *Wind Energy*, vol. 27, no. 3, pp. 258–276, Mar. 2024.

[12] K. H. Chu, J. Pou, S. Ramakrishna, and A. K. Gupta, "Performance of series hybrid excitation synchronous machine in comparison with wound field synchronous machine," in *Proc. Asian Conf. Energy, Power Transp. Electrific. (ACEPT)*, Oct. 2017, pp. 1–6.

[13] K. Kamiev, J. Nerg, J. Pyrhoönen, V. Zaboin, V. Hrabovcovaá, and P. Rafajdus, "Hybrid excitation synchronous generators for island operation," *IET Electr. Power Appl.*, vol. 6, no. 1, pp. 1–11, 2012.

[14] S. Hlioui, Y. Amara, E. Hoang, M. Lecrivain, and M. Gabsi, "Overview of hybrid excitation synchronous machines technology," in *Proc. Int. Conf. Electr. Eng. Softw. Appl.*, Mar. 2013, pp. 1–10.

[15] S. Hlioui, L. Vido, Y. Amara, M. Gabsi, M. Lecrivain, and A. Miraoui, "PM and hybrid excitation synchronous machines: Performances comparison," in *Proc. 18th Int. Conf. Electr. Mach.*, Sep. 2008, pp. 1–6.

[16] D. J. Malcolm and A. C. Hansen, "WindPACT turbine rotor design study," NREL Lab., Tech. Rep., 2006. Accessed: Dec. 27, 2022. [Online]. Available: https://www.nrel.gov/docs/fy06osti/32495.pdf

[17] Y. Amara, G. Barakat, and M. Gabsi, "Comparison of flux control capability of a series double excitation machine and a parallel double excitation machine," in *Proc. IEEE Vehicle Power Propuls. Conf.*, Sep. 2010, pp. 1–6.

[18] A. Ammar, "Modélisation et optimisation d'un générateur synchrone à double excitation de forte puissance," Ph.D. thesis, Ecole Centrale de Lille, Lille, France, 2013. [Online]. Available: https://tel.archives-ouvertes.fr/tel-00907699/document

[19] L. Vido, Y. Amara, and M. Gabsi, *Machines Synchrones à Double Excitation HESM* (Techniques de L'Ingénieur). Revue internationale de génie électrique, 2011. [Online]. Available: https://www.researchgate.net/publication/262356579_Machines_synchrones_a_double_excitation_HESM

[20] W. Xu and M. He, "Novel 6/7 stator/rotor hybrid excitation doubly salient permanent magnet machine," *IEEE Trans. Magn.*, vol. 52, no. 7, pp. 1–5, Jul. 2016.

[21] I. A. A. Afinowi, Z. Q. Zhu, Y. Guan, J. C. Mipo, and P. Farah, "Hybrid-excited doubly salient synchronous machine with permanent magnets between adjacent salient stator poles," *IEEE Trans. Magn.*, vol. 51, no. 10, pp. 1–9, Oct. 2015.

[22] X. Zhao and S. Niu, "Investigation of a new hybrid excitation machine with auxiliary winding for energy recycling," *IEEE Trans. Magn.*, vol. 53, no. 11, pp. 1–5, Nov. 2017.

[23] M. Ahmad and E. Sulaiman, "High torque density design of a new outer-rotor hybrid excitation flux switching machine for in-wheel drive electric vehicle," in *Proc. IEEE Int. Magn. Conf. (INTERMAG)*, May 2015, p. 1.

[24] L. Vido, "Etude d'actionneurs électriques à double excitation destinés au transport: Dimensionnement de structures synchrones," Ph.D. thesis, ENS Cachan, Cachan, France, 2004. [Online]. Available: https://tel.archives-ouvertes.fr/tel-00477166/document

[25] X. Liang, C. Ye, J. Yang, S. Xia, and W. Xu, "Comparison research of a novel brushless hybrid-excitation axial flux machine," in *Proc. 20th Int. Conf. Electr. Mach. Syst. (ICEMS)*, Aug. 2017, pp. 1–5.

[26] Y. Wang and Z. Deng, "Control of a hybrid excitation machine with open-winding structure for hybrid electric vehicles," in *Proc. 17th Int. Conf. Electr. Mach. Syst. (ICEMS)*, Oct. 2014, pp. 2910–2916.

[27] F. Giulii Capponi, G. Borocci, G. De Donato, and F. Caricchi, "Flux regulation strategies for hybrid excitation synchronous machines," *IEEE Trans. Ind. Appl.*, vol. 51, no. 5, pp. 3838–3847, Sep. 2015.

[28] T. K. Hoang, "Design optimization of double excitation synchronous machines in railway traction," Ph.D. thesis, Université Paris-Saclay, Paris, France, 2016.

[29] M. Hendijanizadeh, S. M. Sharkh, and A. A. Qazalbash, "Comparison of PM and hybrid excited machines for marine vessel hybrid-electric propulsion," in *Proc. 13th Int. Conf. Electr. Mach. (ICEM)*, Alexandroupoli, Greece, Sep. 2018, pp. 602–608.

[30] K. Kamiev, A. Parviainen, and J. Pyrhönen, "Hybrid excitation synchronous generators for small hydropower plants," in *Proc. 22nd Int. Conf. Electr. Mach. (ICEM)*, Sep. 2016, pp. 2529–2535.

[31] Y. Ning, C. Liu, R. Jiang, J. Xu, and S. Zhu, "A novel tangential radial hybrid excitation synchronous variable frequency aircraft generator," in *Proc. 15th Int. Conf. Electr. Mach. Syst. (ICEMS)*, Oct. 2012, pp. 1–5.

[32] R. Mbayed, "Contribution to the control of the hybrid excitation synchronous machine for embedded applications," Ph.D. thesis, Université de Cergy Pontoise, Cergy, France, 2014. [Online]. Available: https://tel.archives-ouvertes.fr/tel-00837741/document

[33] A. Boglietti, A. Cavagnino, A. Tenconi, S. Vaschetto, and P. di Torino, "The safety critical electric machines and drives in the more electric aircraft: A survey," in *Proc. 35th Annu. Conf. IEEE Ind. Electron.*, Nov. 2009, pp. 2587–2594.

[34] H. Chakir, H. Ouadi, and F. Giri, "Output feedback control of wind energy conversion system with hybrid excitation synchronous generator," *IFAC-PapersOnLine*, vol. 48, no. 11, pp. 622–627, 2015.

[35] M. Yessef, B. Bossoufi, M. Taoussi, S. Motahhir, A. Lagrioui, H. Chojaa, S. Lee, B.-G. Kang, and M. Abouhawwash, "Improving the maximum power extraction from wind turbines using a second-generation CRONE controller," *Energies*, vol. 15, no. 10, p. 3644, May 2022.

[36] H. Gallas, S. L. Ballois, H. Aloui, and L. Vido, "Modeling, control and grid integration of a 1.5 MW HESG-based wind conversion system," in *Proc. 45th Annu. Conf. IEEE Ind. Electron. Soc. (IECON)*, Oct. 2019, pp. 2416–2421.

[37] A. Akgemci, "Hybrid excited synchronous generator design and comparison of direct drive wind turbines," M.S. thesis, Middle East Tech. Univ., Ankara, Turkiye, 2019.

[38] A. Akgemci and O. Keysan, "Design and analysis of a 2.5 MW hybrid excited synchronous wind turbine generator with two separate rotors," in *Proc. Int. Conf. Electr. Mach. (ICEM)*, vol. 1, Gothenburg, Sweden, Aug. 2020, pp. 1862–1867.

[39] B. Boukhezzar, L. Lupu, H. Siguerdidjane, and M. Hand, "Multivariable control strategy for variable speed, variable pitch wind turbines," *Renew. Energy*, vol. 32, no. 8, pp. 1273–1287, Jul. 2007.

[40] M. Zaibi, G. Champenois, X. Roboam, J. Belhadj, and B. Sareni, "Smart power management of a hybrid photovoltaic/wind stand-alone system coupling battery storage and hydraulic network," *Math. Comput. Simul.*, vol. 146, pp. 210–228, Apr. 2018.

[41] M. Hand, "Variable-speed wind turbine controller systematic designs methodology: A comparison of nonlinear and linear model-based designs," NREL Lab., Tech. Rep., Jul. 1999.

[42] F. D. Bianchi, R. J. Mantz, and C. F. Christiansen, "Gain scheduling control of variable-speed wind energy conversion systems using quasi-LPV models," *Control Eng. Pract.*, vol. 13, no. 2, pp. 247–255, Feb. 2005.

[43] F. D. Bianchi, *Wind Turbine Control Systems: Principles Modeling and Gain Scheduling Design*, 2nd ed. New York, NY, USA: Springer, 2006.

[44] K. Z. Ostergaard, "Robust, gain-scheduled control of wind turbines," Ph.D. thesis, Aalborg Univ., Aalborg, Denmark, 2008.

[45] Z. Wang, Z. Shen, C. Cai, and K. Jia, "Adaptive control of wind turbine generator system based on RBF-PID neural network," in *Proc. Int. Joint Conf. Neural Netw. (IJCNN)*, Jul. 2014, pp. 538–543.

[46] M. Soliman, O. P. Malik, and D. T. Westwick, "Multiple model predictive control for wind turbines with doubly fed induction generators," *IEEE Trans. Sustain. Energy*, vol. 2, no. 3, pp. 215–225, Jul. 2011.

[47] A. Dadone and L. Dambrosio, "Estimator based adaptive fuzzy logic control technique for a wind turbine-generator system," *Energy Convers. Manage.*, vol. 44, no. 1, pp. 135–153, 2003.

[48] S. Bououden, S. Filali, and M. Chadli, "Fuzzy predictive control of a variable speed wind turbine," *Energy Proc.*, vol. 42, pp. 357–366, Jan. 2013.

[49] B. Boukhezzar and H. Siguerdidjane, "Comparison between linear and nonlinear control strategies for variable speed wind turbines," *Control Eng. Pract.*, vol. 18, no. 12, pp. 1357–1368, Dec. 2010.

[50] H. Moradi and G. Vossoughi, "Robust control of the variable speed wind turbines in the presence of uncertainties: A comparison between H_∞ and PID controllers," *Energy*, vol. 90, pp. 1508–1521, Oct. 2015.

[51] Y.-M. Kim, "Robust data driven H-infinity control for wind turbine," *J. Franklin Inst.*, vol. 353, no. 13, pp. 3104–3117, Sep. 2016.

[52] A. Benine-Neto, X. Moreau, and P. Lanusse, "Robust control for an electro-mechanical anti-lock braking system: The CRONE approach," *IFAC-PapersOnLine*, vol. 50, no. 1, pp. 12575–12581, Jul. 2017.

[53] J.-L. Bouvin, X. Moreau, A. Benine-Neto, A. Oustaloup, P. Serrier, and V. Hernette, "CRONE control of a pneumatic self-leveling suspension system," *IFAC-PapersOnLine*, vol. 50, no. 1, pp. 13816–13821, Jul. 2017.

[54] B. Feytout et al., "Maximizing wind turbine production using revisited CRONE control," in *Proc. Eur. Wind Energy Assoc. Conf. (EWEA)*, 2012, p. 1.

[55] B. Feytout, P. Lanusse, J. Sabatier, and S. Gracia, "Robust CRONE design for a variable ratio planetary gearing in a variable speed wind turbine," *Asian J. Control*, vol. 15, no. 3, pp. 806–818, May 2013.

[56] A. Mseddi, S. Le Ballois, H. Aloui, and L. Vido, "Robust control of a wind conversion system based on a hybrid excitation synchronous generator: A comparison between H_∞ and CRONE controllers," *Math. Comput. Simul.*, vol. 158, pp. 453–476, Apr. 2019.

[57] S. El Aimani, "Modélisation de différentes technologies d'éoliennes intégrées dans un réseau de moyenne tension," Ph.D. thesis, Ecole Centrale de Lille, Lille, France, 2004. [Online]. Available: http://l2ep.univ-lille1.fr/fileupload/file/theses/SalmaElAimani.pdf

[58] W. Zheng, Y. Chen, X. Wang, M. Lin, and J. Guo, "Robust fractional order PID controller synthesis for the first order plus integral system," *Meas. Control*, vol. 56, nos. 1–2, pp. 202–214, Jan. 2023.

[59] A. Mseddi, S. Le Ballois, H. Aloui, and L. Vido, "Robust control of a HESG for a wind energy application," *Electr. Power Syst. Res.*, vol. 168, pp. 250–260, Mar. 2019.

[60] A. Mseddi, O. Naifar, and A. Abid, "HESG based WECS overview, modeling, and fractional order control," in *Proc. 20th Int. Multi-Conf. Syst., Signals Devices (SSD)*, Feb. 2023, pp. 591–596.

[61] (May 21, 2023). *NREL Laboratory Forum*. [Online]. Available: https://wind.nrel.gov/forum/wind/viewtopic.php?f=2&t=1818&p=9014&hilit=pitch#p9014

[62] J. Jeong, K. Park, S. Jun, K. Song, and D.-H. Lee, "Design optimization of a wind turbine blade to reduce the fluctuating unsteady aerodynamic load in turbulent wind," *J. Mech. Sci. Technol.*, vol. 26, no. 3, pp. 827–838, Mar. 2012.

[63] G. Boukettaya and O. Naifar, "Improving grid connected hybrid generation system supervision with sensorless control," *J. Renew. Sustain. Energy*, vol. 7, no. 4, 2015.

AMINA MSEDDI received the National Engineering Diploma degree in electrical engineering from the National Engineering School of Sfax, Tunisia, in 2014, the master's degree in computer science, systems, and technology from École Normale Supérieur de Cachan, France, in 2015, and the Ph.D. degree in electrical engineering from the National Engineering School of Sfax, in 2019, in collaboration with the University of Cergy-Pontoise, France. She has been a Postdoctoral Researcher with CEM Laboratory, since September 2022. She is currently engaged in a research project in collaboration with ISE Company. Her research interests include modeling and optimizing double excitation wind generators with a focus on fractional-order, H-infinity, and CRONE controllers.

AHMED ABID received the National Engineering Diploma degree in electrical engineering from the National Engineering School of Sfax, Tunisia, in 2013, and the Ph.D. degree in electrical engineering from the National Engineering School of Sfax, in 2019, in collaboration with University IMS Bordeau, France. In the industrial domain, he has been the Manager Engineer of ISE Company, since 2014. He is currently a member of CEM Laboratory. His research filed includes control systems engineering, electrical engineering, and electronic engineering. His contributions also include works on real-time synthesis of UM shaper, particularly its extension on explicit fractional derivative systems.

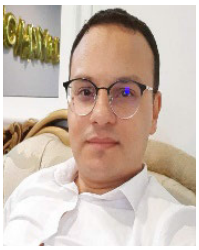

OMAR NAIFAR received the master's degree in computer science from the Faculty of Sciences of Sfax, University of Sfax, Tunisia, in 2010, the Ph.D. degree in electrical engineering, in 2015, and the H.D.R. degree in electrical engineering from the National School of Engineering, Sfax, in 2021. His master's project in automatic and industrial computing from the National School of Engineering, in 2012. He is currently a member with the Control and Energy Management Laboratory (CEM-Lab), Department of Electrical Engineering, National School of Engineering. His research interests include robust nonlinear control (higher-order sliding mode, backstepping, and adaptive control), theoretical aspects of nonlinear observer design, control and fault diagnosis, and fractional-order control systems. He is an Associate Editor of the international journal *Asian Journal of Control* (Wiley) indexed by the Web of Science Clarivate Database.

MOHAMED RHAIMA was born in 1984. He received the M.Sc. degree in mathematics from the Faculty of Sciences of Tunis, Tunisia, in 2012, and the joint Ph.D. degree in mathematics from the University of Tunis El Manar, Tunisia, and the Tor Vergata University of Rome, Rome, Italy, in 2017. His research interests include nonlinear stochastic control systems, nonlinear stochastic dynamical systems, stochastic fractional-order systems, and stochastic delay systems.

ABDELLATIF BEN MAKHLOUF received the bachelor's and master's degrees in mathematics from the Department of Mathematics, University of Sfax, Tunisia, and the Ph.D. degree in mathematics from the University of Sfax, in 2015. Currently, he is an Associate Professor of mathematics with the University of Sfax. His current research interests include fractional differential equations, ordinary differential equations, stochastic differential equations, control theory, and stability theory.

LASSAAD MCHIRI received the bachelor's and master's degrees in mathematics from the Department of Mathematics, University of Tunis El Manar, Tunisia, and the Ph.D. degree in mathematics from the University of Sfax, Tunisia, in 2016. Currently, he is an Assistant Professor of mathematics with Panthéon-Assas University Paris II, France. His current research interests include fractional differential equations, ordinary differential equations, stochastic differential equations, control theory, and stability theory.